Characterization of Aluminophosphate-Based Tubular Mesoporous Molecular Sieves

Zhaohua Luan,[†] Dongyuan Zhao,[†] Heyong He,[‡] Jacek Klinowski,[‡] and Larry Kevan*[,†]

Department of Chemistry, University of Houston, Houston, Texas 77204-5641, and
Department of Chemistry, University of Cambridge, Lensfield Road, Cambridge CB2 1EW, U.K.

Received: September 25, 1997

A series of aluminophosphate-based tubular mesoporous molecular sieves without (UHM-1) and with substituted silicon (UHM-3) have been synthesized at room temperature in the presence of a cationic surfactant cetyltrimethylammonium chloride (CTACl) and an organic base tetramethylammonium hydroxide (TMAOH). Characterization by powder X-ray diffraction (XRD), electron probe microanalysis (EPMA), transmission electron microscopy (TEM), N_2 adsorption, and ^{27}Al, ^{31}P, and ^{29}Si magic-angle-spinning (MAS) NMR spectroscopies has been carried out to understand both the pore structures and the local atomic arrangements of these solid products. The synthesis of UHM-1 and UHM-3 is successful only at room temperature within the following molar gel composition: Al_2O_3:(0.6−3.4) P_2O_5:(0.0−1.0) SiO_2:(0.24−0.50) CTACl:(8.5−47.0) TMAOH:(200−642) H_2O. The presence of TMAOH is essential to maintain the gel pH at 8.5 or above. The pH greatly influences the nature of the final "crystalline" products, particularly the coordination of aluminum and phosphorus. XRD, EPMA, TEM, and N_2 adsorption measurements show that these solid products have a unique composition and disordered tubular mesopores with an average pore diameter of about 35 Å in the calcined form. The overall P/Al ratio of UHM-1 is less than unity, especially in gels of higher pH, indicating incomplete condensation of phosphorus and a nonideal aluminophosphate framework. This may account for their poorer thermal stability relative to microporous aluminophosphate molecular sieves and aluminosilicate-based MCM-41 materials. ^{27}Al and ^{31}P MAS NMR reveal that aluminum in UHM-1 with a P/Al ratio of 0.60 synthesized at a gel pH of 8.5 is present in both tetrahedral and octahedral environments while phosphorus is present in a tetrahedral environment and also as hydroxylated species. As the P/Al ratio of UHM-1 decreases together with increasing gel pH, the relative amounts of tetrahedral aluminum and tetrahedral phosphorus decrease. This change suggests some Al−O−P linkages in the tetrahedral regions of the UHM-1 samples, and an increasing octahedral aluminum content at lower P/Al ratio indicates that octahedral aluminum alone can construct a tubular mesoporous structure. After incorporation of silicon into UHM-1, ^{29}Si, ^{27}Al, and ^{31}P MAS NMR of UHM-3 reveal that silicon is atomically dispersed and that the relative amounts of tetrahedral aluminum and tetrahedral phosphorus increase monotonically with increasing silicon incorporation. Virtually all the aluminum is tetrahedral, and all the phosphorus is tetrahedral after silicon incorporation reaches a Si/Al ratio of unity. This indicates more ordered atomic arrangements of tetrahedral silicon, aluminum, and phosphorus via oxygen bridges in UHM-3 than in UHM-1. The incorporation of silicon appears to make the aluminophosphate framework more flexible and facilitates the formation of an aluminophosphate-based mesoporous structure.

Introduction

There has been an important breakthrough with the discovery of a new family of aluminosilicate-based mesoporous molecular sieves designated as M41S,[1,2] which dramatically extends the concept of traditional molecular sieves beyond the realm of zeolites and aluminophosphates. These novel mesoporous materials are synthesized under mild hydrothermal conditions from gels containing sources of silicon, aluminum, and a long-chain organic structure-directing agent, and the formation of these inorganic mesoporous structures is assumed to proceed via a liquid crystal templating mechanism.[1−3] MCM-41, the hexagonal member of this family of materials, possesses uniform mesopore channels varying from about 15 to 100 Å and has stimulated interest in the potential use of these materials as catalysts for large molecule transformations, which have been reviewed recently by Sayari.[4]

Like zeolites, aluminophosphate molecular sieves ($AlPO_4$-*n*), which are constructed by aluminum and phosphorus tetrahedra, are also extensively studied crystalline microporous materials.[5] Correspondingly, several research groups have attempted to prepare aluminophosphate-based mesoporous molecular sieves. Oliver et al.[6] and Sayari et al.[7−9] employed a high-temperature (100−180 °C) hydrothermal process to achieve this goal in a water-free tetraethylene glycol solvent and in water, respectively. In both of these approaches, a neutral surfactant, such as decylamine or dodecylamine, is used as a structure-directing agent, and Catapal B alumina and phosphoric acid are used as the aluminum and phosphorus sources. However, these methods lead to a lamellar phase with poor thermal stability although some modified routes based on these syntheses have been recently reported.[10−13] A tubular mesoporous aluminophosphate phase, which is structurally similar to MCM-41 and has improved thermal stability, has been reported most recently by the Houston laboratory[14,15] and from

[†] University of Houston.
[‡] University of Cambridge.

S1089-5647(97)03109-X CCC: $15.00
Published on Web 01/22/1998

some other groups.[16−18] In contrast to previous approaches, these latter studies use a cationic alkylamine surfactant as a structure-directing agent and conduct the synthesis at room temperature and in basic aqueous solution. In another approach,[19] ordered nonlamellar mesoporous aluminophosphate and galloaluminophosphate materials were synthesized by reacting a buffered hydrogen phosphate/dihydrogen phosphate solution with a layered mesoscopic salt of $AlO_4Al_{12}(OH)_{24}(H_2O)_{12}^{7+}$ and $GaO_4Al_{12}(OH)_{24}(H_2O)_{12}^{7+}$ tridecamers in the presence of sodium dodecyl sulfate anionic surfactant.

More complete characterization of the pore structure and the local atomic arrangements of aluminum and phosphorus in this tubular mesoporous aluminophosphate phase requires a combination of various techniques. In addition to X-ray diffraction (XRD) and transmission electron microscopy (TEM) which have been mostly used in previous works to identify the presence of the tubular mesoporous phase,[14−18] low-temperature N_2 adsorption isotherms can provide additional information about the mesoporous structure in terms of the specific surface area, pore volume, and mesopore size distribution.[20,21] Solid-state magic-angle-spinning (MAS) NMR spectroscopy can give important information about the coordination environments of magnetic nuclei like aluminum and phosphorus.[22−24]

In this work we report complete synthetic details of the preparation of aluminophosphate-based tubular mesoporous molecular sieves UHM-1 together with comprehensive characterization of this material. Since the incorporation of silicon into the framework of microporous aluminophosphate $AlPO_4$-*n* molecular sieves can create Brønsted acidity for possible catalytic application of these materials, silicon-substituted UHM-3 material is also studied. In addition, the synthesis is generalized based on the electrostatic complementarity between the inorganic ions in solution and the charged surfactant headgroups developed by Monnier et al. for the formation of mesoporous aluminosilicate-based MCM-41 materials.[25]

Experimental Section

Synthesis. Both aluminophosphate UHM-1 and silicoaluminophosphate UHM-3 were synthesized at room temperature using cetyltrimethylammonium chloride (CTACl, Aldrich, 25% in water) as a structure-directing agent and aluminum hydroxide (53.5 wt % Al_2O_3, USP Pfaltz & Bauer Inc.), phosphoric acid (85 wt %, EM Industries), and tetraethyl orthosilicate (TEOS, Aldrich) as aluminum, phosphorus, and silicon sources, respectively. Generally, this synthesis can be conducted in gels within a broad range of molar compositions: Al_2O_3:(0.6−3.4) P_2O_5:(0.0−1.0) SiO_2:(0.24−0.50) CTACl:(8.5−47.0) TMAOH:(200−642) H_2O. A typical synthesis procedure at a P/Al ratio of 1.00 for aluminophosphate UHM-1 can be described as follows: 3.53 g of aluminum hydroxide was slowly added into a solution of 4.2 g of phosphoric acid dispersed in 65 g of water under vigorous stirring. The mixture was then combined with 11.6 g of CTACl and 50 g of water with stirring. After 2 h about 17−40 g of tetramethylammonium hydroxide (TMAOH, Aldrich, 25 wt % in water) was slowly added dropwise into the above mixture until a pH value in the range 8.5−14.0, which determines the P/Al ratio of the solid product (see below), was reached. The gel was then stirred for 72 h at room temperature. The solid product was filtered, repeatedly washed with deionized water, and dried in air. These aluminophosphate UHM-1 samples are designated as UHM-1-(*X*), where *X* is the P/Al ratio in the solid product. For the synthesis of silicon-substituted silicoaluminophosphate UHM-3, the same procedure was employed, except that the synthesis was performed at a P/Al ratio of 2.00 by doubling the amount of phosphoric acid and at a constant pH value of 8.5. An amount of TEOS for a desired Si/Al ratio was added with stirring into the gel mixture before the addition of TMAOH. These solid products generally have a similar P/Al ratio (see below) and are designated as UHM-3-(*Y*), where *Y* is the Si/Al ratio in the solid product. Table 1 gives conditions for these typical syntheses described above.

TABLE 1: Synthesis Conditions and Elemental Compositions of the Gel Mixtures and Solid Products for UHM-1 and UHM-3 Materials

	gel mixture			solid product	
sample	pH	P/Al	Si/Al	P/Al	Si/Al
UHM-1-(0.60)	8.5	1.00		0.60	
UHM-1-(0.37)	9.5	1.00		0.37	
UHM-1-(0.23)	10.0	1.00		0.23	
UHM-1-(0.18)	14.0	1.00		0.18	
UHM-3-(0.10)	8.5	2.00	0.10	0.68	0.10
UHM-3-(0.26)	8.5	2.00	0.25	0.75	0.26
UHM-3-(0.52)	8.5	2.00	0.50	0.63	0.52
UHM-3-(1.01)	8.5	2.00	1.00	0.71	1.01

The organic structure-directing agent in the pores of these samples was removed by heating a sample at increasing temperature steps between 200 and 500 °C for 5 h at each step in flowing nitrogen and, finally, by calcination at 500 °C for 6 h in flowing oxygen.

Characterization. Electron probe microanalysis (EPMA) was performed on a JEOL JXA-8600 spectrometer. Table 1 gives the elemental composition of some typical samples.

Powder XRD patterns were collected using a Philips 1840 powder diffractometer with Cu Kα radiation (40 kV, 25 mA) at 0.025° step size and 1 s step time over the range $1.5° < 2\theta < 15°$. The samples were prepared as thin layers on metal slides.

For TEM observation, powder specimens were preground and deposited on a grid with a holey carbon film and rapidly transferred to a JEOL 2000 FX electron microscope with an accelerating voltage of 100 kV.

N_2 adsorption isotherms were measured at 77 K using a Micromeritics Gemini 2375 analyzer. The volume of adsorbed N_2 was normalized to standard temperature and pressure (STP). Prior to the experiments, samples were dehydrated at 250 °C for 5 h. The specific surface area, A_{BET}, was determined from the linear part of the BET equation ($P/P_0 = 0.05-0.31$). The calculation of the pore size distribution was performed using the desorption branches of the N_2 adsorption isotherms and the Barrett−Joyner−Halenda (BJH) formula.[26] The cumulative mesopore (17−100 Å) surface area, A_{BJH}, was obtained from the pore size distribution curves.

Solid-state NMR spectra were recorded at 9.4 T using a Chemagnetics CMX-400 spectrometer. ^{29}Si MAS spectra were measured at 79.45 MHz with 60° pulses and 600 s recycle delays using zirconia rotors 7.5 mm in diameter spun at 3 kHz. ^{27}Al MAS spectra were measured at 104.3 MHz with 0.3 s recycle delays using zirconia rotors 4 mm in diameter spun at 8 kHz and corrected by subtracting the empty rotor spectrum. Short $\pi/20$ radio-frequency pulses were used to ensure reliability. ^{31}P Bloch decay MAS and ^{1}H−^{31}P cross-polarization (CP)/MAS NMR spectra were recorded at 161.9 MHz using a MAS probehead with zirconia rotors 4 mm in diameter. ^{31}P MAS spectra were recorded with spinning at about 8 kHz, 90° pulses of 3 μs duration, and 45 s recycle delays. ^{1}H−^{31}P CP/MAS NMR spectra were recorded with spinning at about 6 kHz, 4 μs ^{1}H 90° pulses, 4 ms contact times, and 4 s recycle delays. The chemical shifts are given in ppm from external tetramethylsilane (TMS) for ^{29}Si, $Al(H_2O)_6^{3+}$ for ^{27}Al, and 85% H_3PO_4 for ^{31}P.

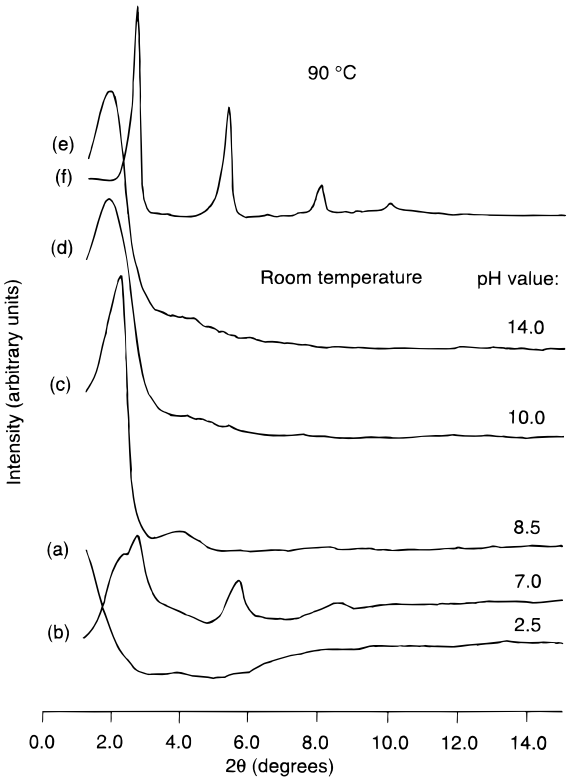

Figure 1. Powder XRD patterns of as-synthesized aluminophosphate UHM-1 samples prepared at room temperature in gels with variable pH values: (a) 2.5, (b) 7.0, (c) 8.5, (d) 10.0, and (e) 14.0. (f) shows the powder XRD pattern of as-synthesized aluminophosphate prepared in the same gel as (c) but at the increased temperature of 90 °C.

Results

Synthesis and Powder X-ray Diffraction. *Aluminophosphate UHM-1*. Figure 1 shows powder XRD patterns of the solid products obtained from gels with a fixed P/Al ratio of 1.00 but with variable amounts of TMAOH, which is used as a base to adjust the gel pH value. At acidic condition (pH < 7), XRD shows that the resultant solid product lacks any defined structure (Figure 1a), indicating an amorphous nature of this material. As synthesis is performed at neutral condition (pH 7.0), the solid product obtained gives four XRD peaks at 2.2°, 2.8°, 5.6°, and 8.5° of 2θ angle (Figure 1b). The relative intensities and repeat distances of the latter three intense peaks suggest that a lamellar phase with $d(100)$ spacing of about 35 Å dominates this sample (unit cell parameter $a_0 = 2d(100)/\sqrt{3}$).[6−13] As the gel pH increases to 8.5, a well-defined XRD pattern with a prominent peak at 2.2° 2θ and some broad but clearly present peaks in the 2θ range of 3.0°−8.0° are observed (Figure 1c). This XRD pattern is similar to that of siliceous MCM-41 materials[1,2] and can be indexed to a hexagonal lattice with a $d(100)$ spacing of about 40 Å, indicating a successful synthesis of aluminophosphate-based hexagonal mesoporous material. However, as compared to siliceous MCM-41,[1,2] the diffraction peak corresponding to a $d(100)$ spacing of about 40 Å and the other three diffraction peaks due to (110), (200), and (210) reflections of a hexagonal lattice are broadened and are not as well resolved. The same broadening of XRD peaks has been observed previously for aluminosilicate MCM-41[21] and HMS, a siliceous MCM-41 analogue synthesized via a neutral-templating route,[27] and has been interpreted as due to finite size effects of a very fine particle morphology rather than due to a more disordered hexagonal framework structure. This is also the case for disordered mesoporous silica materials MSU-1, synthesized by a neutral assembly pathway using nonionic poly(ethylene oxide) surfactant,[28] KIT-1, prepared via an electrostatic templating route in the presence of ethylenediaminetetraacetic acid tetrasodium salt ($EDTANa_4$),[29] and also an alumina mesoporous material synthesized by reacting aluminum alkoxides and carboxylic acids with controlled amounts of water in alcoholic solvents.[30] The pore structure of these materials is believed to be a three-dimensional, disordered network of short, wormlike, tubular channels while the channel widths are uniform. Since TEM images from UHM-1 also show a large disorder (see transmission electron microscopy below), the latter interpretation may account for our XRD results. At higher pH values of 10.0−14.0, the solid products obtained give even broader XRD patterns than at pH 8.5 and a larger $d(100)$ spacing of about 44.5 Å (Figure 1d,e), indicating some change in the structure and composition (also see electron probe microanalysis below). These results clearly show that UHM-1 can be formed only in basic media (Table 1).

Figure 1f shows the XRD pattern of a solid product obtained from the same gel as for the sample with the XRD pattern of Figure 1c but at an increased synthesis temperature of 90 °C. The presence of only diffraction peaks that are higher orders of the first (001) peak suggests a well-defined but unstable lamellar phase (UHM-2). This aluminophosphate mesoporous phase has been studied by Sayari et al.[6−13]

Silicoaluminophosphate UHM-3. Incorporation of silicon into UHM-1 to form UHM-3 is successful up to a Si/Al ratio of unity under the same conditions for UHM-1 formation. XRD patterns of the UHM-3 samples with variable Si/Al ratio in this range synthesized at pH 8.5 are similar to those of UHM-1 samples synthesized also at pH 8.5 (Figure 1c).

Heat Treatment. As these as-synthesized UHM-1 and UHM-3 samples are subjected to heat treatment to decompose the organic structure-directing agent, the resolution of their XRD patterns deteriorates as the temperature goes up, especially over 300 °C (Figure 2a−d). This indicates the occurrence of a framework rearrangement of the tubular mesopores into a less ordered structure upon removing the organic structure-directing agent by heat treatment. However, the integrity of the tubular mesoporous structures of UHM-1 and UHM-3 is retained even after complete decomposition of the organic structure-directing agent by calcination at 500 °C in flowing oxygen for 6 h (Figure 2e) (also see N_2 adsorption measurement below).

Electron Probe Microanalysis. EPMA analysis shows that both as-synthesized UHM-1 and UHM-3 have a unique composition; therefore, the formation of either pure phase Al_2O_3 or P_2O_5 can be excluded. However, the overall P/Al ratios of all samples are much less than unity, especially the samples synthesized with higher gel P/Al ratios (Table 1). This indicates that some aluminum species are involved independently in the mesoporous material assembly without a neighbor phosphorus due to incomplete condensation. This suggests that these UHM-1 and UHM-3 materials possess a nonideal three-dimensional aluminophosphate framework different from microporous aluminophosphate molecular sieves.[31]

The analysis of UHM-3 confirms that silicon is homogeneously distributed over a UHM-3 solid particle and that the overall Si/Al ratio of UHM-3 is comparable with that in the initial gel mixture (Table 1).

Transmission Electron Microscopy. The tubular channels of about 40 Å in diameter in UHM-1 and UHM-3 samples are directly visible in the TEM images illustrated in Figure 3 for typical as-synthesized samples. However, as compared to previously reported TEM images for siliceous MCM-41 materi-

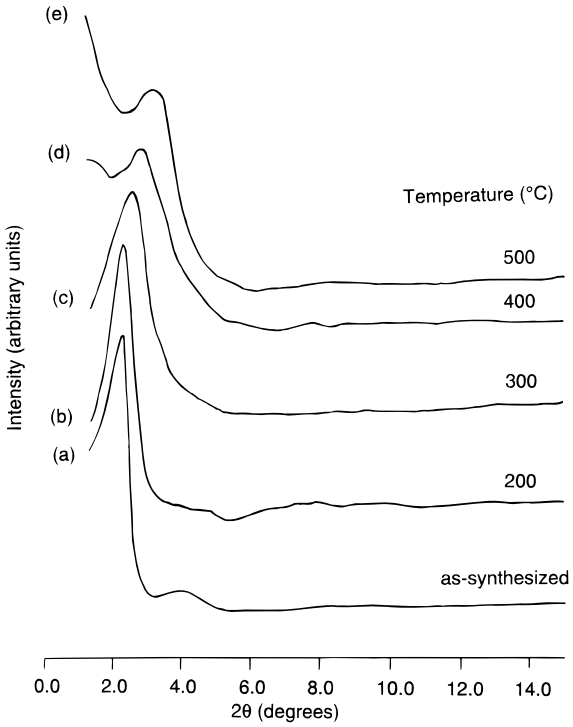

Figure 2. Powder XRD patterns of aluminophosphate sample UHM-1-(0.60) after being subjected to heat treatment in flowing nitrogen for 5 h at increasing temperature: (a) as-synthesized, (b) 200, (c) 300, (d) 400, and (e) 500 °C. Following heat treatment at 500 °C in nitrogen further calcination of the sample at 500 °C in flowing oxygen for 6 h does not affect the XRD pattern.

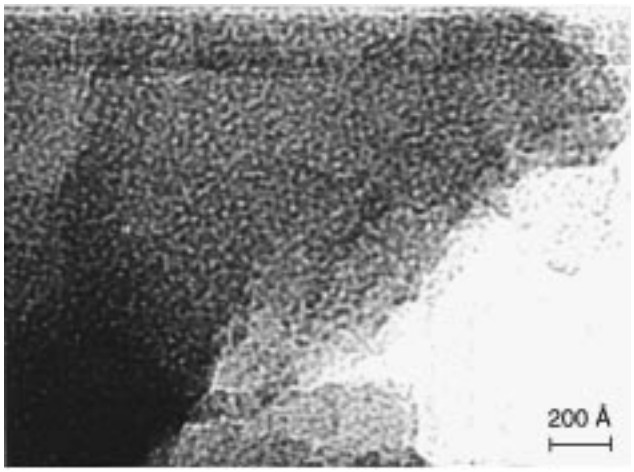

Figure 3. TEM image of as-synthesized aluminophosphate sample UHM-1-(0.60).

als,[1,2] the TEM images from UHM-1 and UHM-3 show a large disorder in the mesopore shape, which is similar to those from MSU-1[28] and KIT-1 materials.[29] This result suggests that UHM-1 and UHM-3 possess a disordered tubular mesoporous structure consistent with the XRD patterns.

N_2 Adsorption Measurement. *BET Specific Surface Area.* Following heat treatment in flowing nitrogen at increasing temperature for removal of the organic structure-directing agent, multipoint BET specific surface areas, A_{BET}, of typical UHM-1 and UHM-3 samples are presented in Figure 4. The BET specific surface areas of these samples increase with increasing heat treatment temperature and reach maxima in the range 450−700 m^2/g around 400 °C and then decrease somewhat upon heating to the higher temperature of 500 °C. Following this

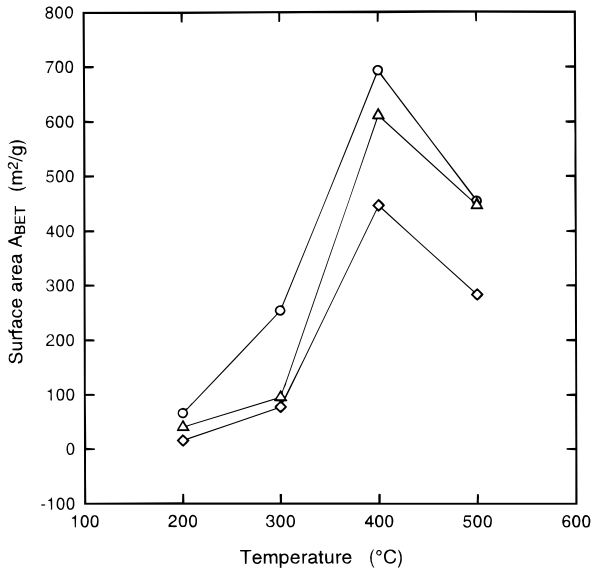

Figure 4. Specific BET surface areas of aluminophosphate UHM-1 and silicoaluminophosphate UHM-3 samples after being subjected to heat treatment in flowing nitrogen at increasing temperature: (○) UHM-1-(0.18), (△) UHM-3-(1.01), (◇) UHM-1-(0.60).

heat treatment at 500 °C, further calcination of the sample at 500 °C in flowing oxygen for 6 h does not much affect their BET specific surface areas. Obviously, the organic structure-directing agent starts to decompose at temperatures above 200 °C and is complete at 400−500 °C. The high BET specific surface areas to 700 m^2/g after treatment at 400 °C strongly support the XRD and TEM results that these UHM-1 and UHM-3 samples possess a relatively stable tubular mesoporous structure rather than a lamellar configuration. The small decrease of the BET specific surface areas at 500 °C indicates a partial framework collapse and thus lower thermal stability in comparison with siliceous MCM-41. In addition, the changes in the BET specific surface areas with increasing heat treatment temperature seem independent of the P/Al or Si/Al ratios.

N_2 Adsorption Isotherms. Figure 5 shows typical N_2 adsorption isotherms from calcined UHM-1 and UHM-3 samples. Both give typical irreversible type IV adsorption isotherms with an H1 hysteresis loop as defined by IUPAC.[32] N_2 adsorption at low relative pressure ($P/P_0 < 0.31$) is accounted for by monolayer adsorption of N_2 on the walls of the mesopores and does not imply the presence of micropores. As the relative pressure increases ($P/P_0 > 0.31$), the isotherms exhibit sharp inflections in the P/P_0 range from 0.45 to 0.75 characteristic of capillary condensation within uniform mesopores. The P/P_0 position of the reflection points is clearly related to a diameter in the mesopore range, and the sharpness of these steps indicates the uniformity of the mesopore size distribution.

Given the different degrees of spontaneity of the adsorption−desorption process, the hysteresis loop in type IV N_2 adsorption isotherms provides further information about the mesopore structure. The broad hysteresis loop in the isotherms of UHM-1 and UHM-3 reflects some mesopore disorder in shape, which limits the emptying and filling of the accessible volume. This is also consistent with the XRD and TEM results. Comparing UHM-1 and UHM-3 samples, the latter (Figure 5a) exhibits a little sharper inflection in its isotherm than the former (Figure 5b), indicating a less disordered mesoporous structure after silicon incorporation.

Pore Size Distribution. The pore size distribution can be calculated from the Kelvin equation. Tanev et al.[20] claimed

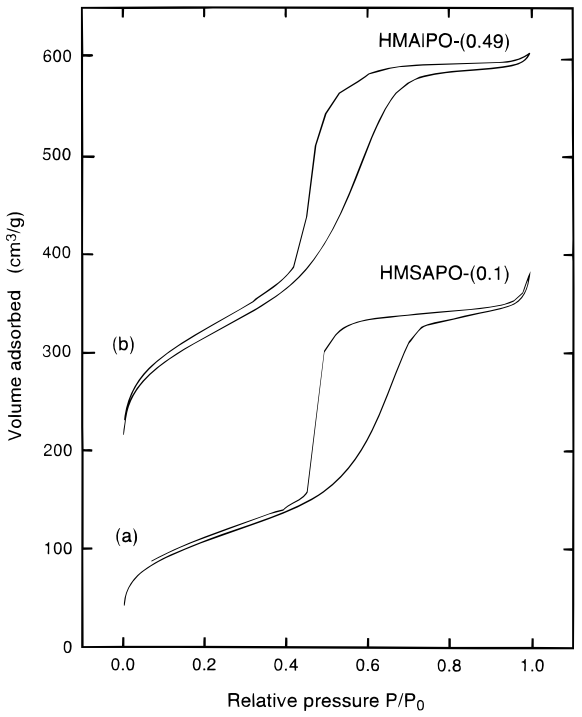

Figure 5. Adsorption−desorption isotherms of nitrogen at 77 K: (a) calcined silicoaluminophosphate sample UHM-3-(0.10) and (b) calcined aluminophosphate sample UHM-1-(0.49)

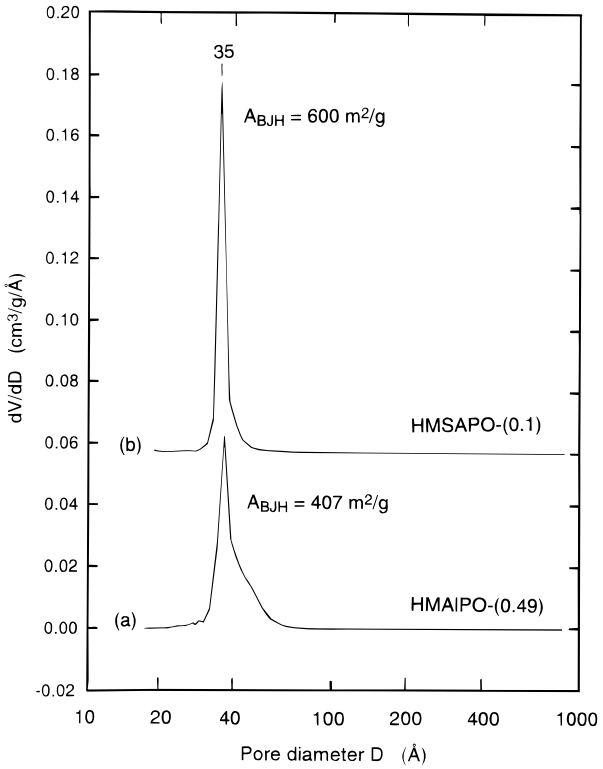

Figure 6. Pore size distribution curves for (a) calcined aluminophosphate UHM-1-(0.49) and (b) calcined silicoaluminophosphate UHM-3-(0.10).

that the desorption branch of N_2 adsorption isotherms carries more information about the degree of pore blocking than does the adsorption branch and demonstrated that the BJH computation procedure based on the desorption branch can be satisfactorily applied in practice for mesoporous materials. Our calculations are based the on these arguments, and the results are presented in Figure 6 for typical samples. A BJH plot for the physisorption of N_2 on a UHM-1 sample leads to a little broader pore size distribution than in UHM-3 with a mesopore size of about 35 Å and a mesopore surface area A_{BJH} of 407 m^2/g. In contrast, a BJH plot for the physisorption of N_2 on a UHM-3 sample leads to a relatively narrower pore size distribution with a pore size of about 35 Å and a higher mesopore surface area A_{BJH} of 600 m^2/g, indicating that silicon incorporation enhances the formation of a mesoporous aluminophosphate structure. These results directly confirm the presence of tubular mesoporous channels in UHM-1 and UHM-3 materials. The approximate pore size calculation by nitrogen physisorption is smaller than the repeat distance $a_0 = 46$ Å determined by XRD ($a_0 = 2d(100)/\sqrt{3}$, where $d(100) = 40$ Å for typical samples), because the latter includes the thickness of the pore wall. Thus, we can estimate that the pore walls of these UHM-1 and UHM-3 materials are around 11 Å thick.

^{27}Al MAS NMR. *Aluminophosphate UHM-1.* Figure 7 shows ^{27}Al MAS NMR spectra of as-synthesized UHM-1 materials. The spectrum from the sample with a relatively high P/Al ratio of 0.60 gives two resolved lines at 43 and 1 ppm (Figure 7a). Based on extensive literature reports on various microporous aluminophosphate $AlPO_4$-*n* materials,[22,23,33,34] the line at 43 ppm can be assigned to aluminum in a tetrahedral environment (AlO_4 structural unit), in which aluminum is covalently bound to four P atoms via oxygen bridges, and the chemical shift at 1 ppm can be assigned to octahedral aluminum (AlO_6 structural unit). As the overall P/Al ratio decreases, the line at 43 ppm corresponding to tetrahedral aluminum decreases

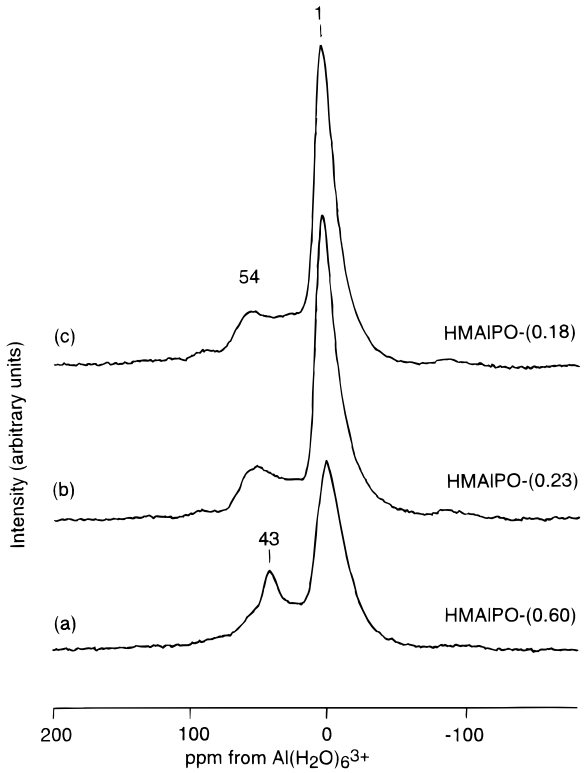

Figure 7. ^{27}Al MAS NMR spectra of as-synthesized aluminophosphate samples (a) UHM-1-(0.60), (b) UHM-1-(0.37), and (c) UHM-1-(0.18).

in intensity and shifts slightly to 54 ppm, which is also characteristic of tetrahedral aluminum,[24] but the line at 1 ppm increases in intensity without any change in chemical shift (Figure 7b,c), indicating a dependence of the amount of tetrahedral aluminum on phosphorus incorporation. These

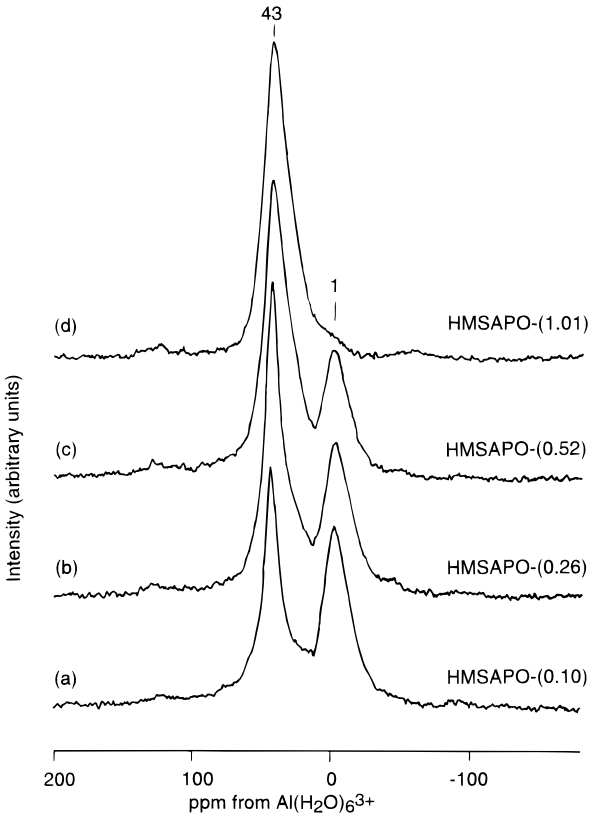

Figure 8. ^{27}Al MAS NMR spectra of as-synthesized silicoaluminophosphate samples (a) UHM-3-(0.10), (b) UHM-3-(0.26), (c) UHM-3-(0.52), and (d) UHM-3-(1.01).

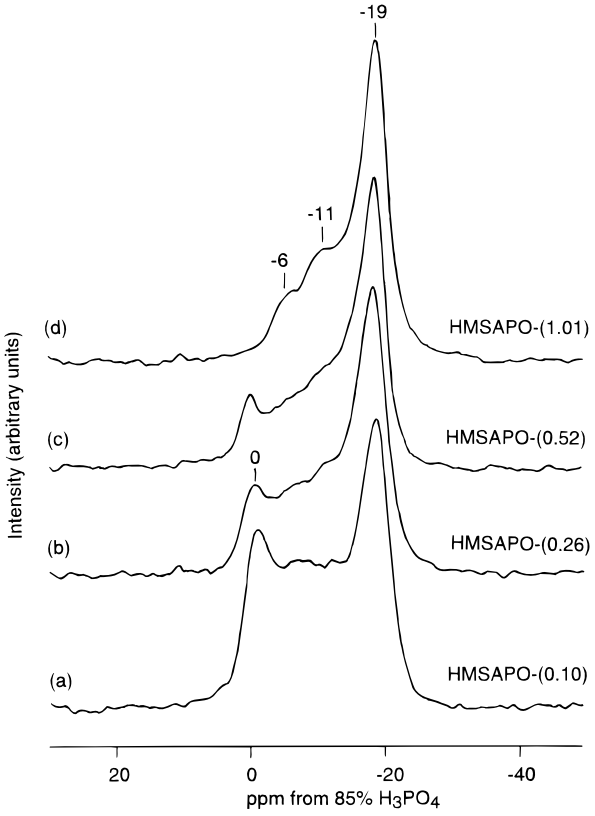

Figure 9. ^{31}P MAS NMR spectra of as-synthesized silicoaluminophosphate samples (a) UHM-3-(0.10), (b) UHM-3-(0.26), (c) UHM-3-(0.52), and (d) UHM-3-(1.01).

results clearly show the simultaneous presence of both AlO_4 and AlO_6 structural units in UHM-1 corresponding to the deviation of the overall P/Al ratio from unity and indicate that the AlO_6 structural unit alone can build a tubular mesoporous structure.[30]

Silicoaluminophosphate UHM-3. Incorporation of silicon into UHM-1 substantially modifies the local atomic environment for aluminum, as shown in the ^{27}Al MAS NMR spectra of UHM-3 in Figure 8. The line at 43 ppm corresponding to tetrahedral aluminum exhibits a larger intensity than the 1 ppm line of octahedral aluminum even at low silicon loading (Figure 8a). With increasing silicon incorporation the 43 ppm line increases in intensity, whereas the 1 ppm line decreases (Figure 8a−c), and as the silicon loading approaches a Si/Al ratio of 1.01, only the 43 ppm line can be resolved. This result indicates that the incorporation of silicon promotes a more ordered arrangement of the aluminophosphate framework.

^{31}P MAS NMR. *Silicoaluminophosphate UHM-3*. To assign various phosphorus environments, ^{31}P MAS NMR spectra of UHM-3 rather than UHM-1 are shown first in Figure 9, since it gives better resolved lines. A UHM-3 sample with a low Si/Al ratio of 0.10 exhibits two intense lines at −19 and 0 ppm and two other weak lines at −6 and −11 ppm which overlap with the −19 and 0 ppm lines (Figure 9a). However, a direct assignment for these resonances requires care because the ^{31}P MAS NMR spectra of UHM-3 show a considerable downfield shift in comparison with those of microporous aluminophosphate $AlPO_4$-*n* materials. In the literature, most of the reported chemical shifts of ^{31}P in microporous $AlPO_4$-*n* materials fall in the range −19 to −30 ppm and are attributed to tetrahedral phosphorus (PO_4 structural unit) covalently linked via four oxygen bridges to aluminum.[22,23,33−35] The only reported ^{31}P chemical shifts that fall in the range 0 to −19 ppm are from mesoporous lamellar materials by Sayari et al.,[7−9] who claimed that such a downfield shift of the ^{31}P NMR signal is caused by several factors including the number of surrounding aluminums and/or the nature of the ligands in the second coordination sphere of phosphorus. This means that the presence of either acid protons or ammonium cations or coordinated water may cause a downfield chemical shift of ^{31}P. In addition, it has also been established that the ^{31}P signals are further downfield for phosphorus species containing highly coordinated aluminum than for those containing only 4-coordinated aluminum.[36] For tubular mesoporous aluminophosphate-based materials UHM-1 and UHM-3, highly coordinated aluminum does occur as already shown by ^{27}Al MAS NMR. To further verify the local environments of phosphorus in UHM-3, ^{1}H−^{31}P cross polarization (CP) with MAS was applied to the same sample, and the result is given in Figure 10b. This shows that the line at 0 ppm is greatly enhanced by ^{1}H−^{31}P CP, but this influence becomes less pronounced for the lines with increasing chemical shift. A similar spectroscopic result has been reported previously for gallophosphate molecular sieves and has been attributed to the existence of hydroxylated phosphorus.[37] Obviously, there are several distinct chemical environments for phosphorus in this UHM-3 sample in which a variable number of protons are present in the second coordination sphere of phosphorus. On the basis of these experiments and the arguments mentioned above, we can assign the ^{31}P MAS NMR lines in Figure 9a as follows. The occurrence of the ^{31}P chemical shift at −19 ppm is due to tetrahedral phosphorus bonded to four aluminums via oxygen bridges, as a $P(OAl)_4$ unit, whereas the lines at −11, −6, and 0 ppm are assigned to phosphorus atoms with mixed coordination $P(OH)_x(OAl)_{4-x}$, where x is 1−3. This interpretation supports that there is no strict aluminum and phosphorus ordering of alternating AlO_4

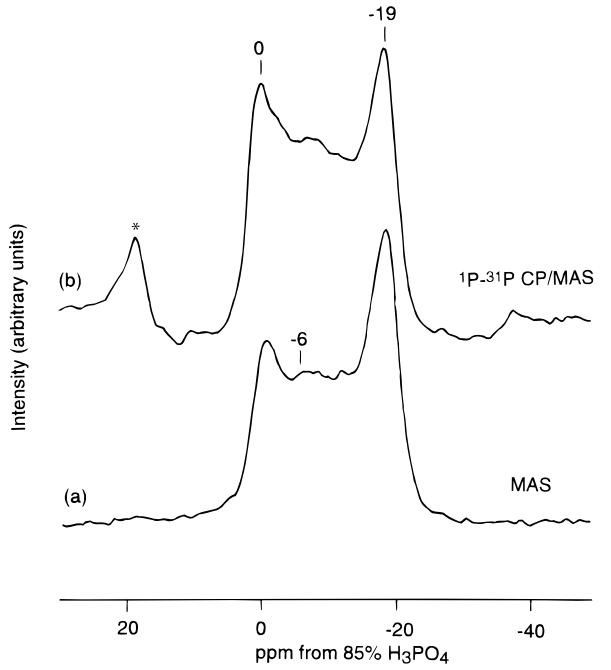

Figure 10. (a) ^{31}P MAS NMR and (b) ^{1}H−^{31}P CP/MAS NMR spectra of as-synthesized silicoaluminophosphate samples UHM-3-(0.10). The asterisk denotes a spinning sideband.

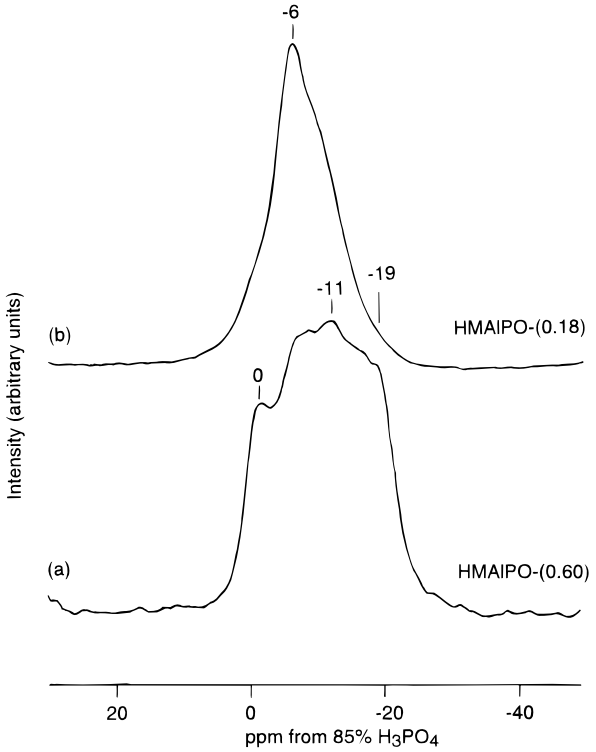

Figure 11. ^{31}P MAS NMR spectra of as-synthesized aluminophosphate samples (a) UHM-1-(0.60) and (b) UHM-1-(0.18).

and PO_4 structural units in these aluminophosphate-based tubular mesoporous materials for UHM-1 and UHM-3 with low silicon loading.

However, with increasing silicon incorporation in UHM-3, the three lines at 0, −6, and −11 ppm corresponding to phosphorus with variable numbers of hydroxyl ligands show less intensity relative to the −19 ppm line due to the $P(OAl)_4$ unit (Figure 9a−c). As the silicon loading approaches a Si/Al ratio of unity, the ^{31}P MAS NMR spectrum becomes dominated by the line at −19 ppm. The incorporation of silicon into UHM-1 seems to facilitate the formation of a more ordered aluminophosphate-based tubular mesoporous structure.

Aluminophosphate UHM-1. Without substituted silicon UHM-1 gives a ^{31}P MAS NMR spectrum with a very broad shape over the range from 0 to −20 ppm, but the four lines at 0, −6, −11, and −19 ppm corresponding to different coordination environments of phosphorus as $P(OH)_x(OAl)_{4-x}$, where x is 1−4, still can be identified (Figure 11a). However, the first three lines show a larger intensity as compared to UHM-3, suggesting more incomplete condensation of PO_4 units and more disorder in UHM-1 than in UHM-3.

As the P/Al ratio decreases to 0.18, the −19 ppm line decreases in intensity and almost disappears as do the lines at 0 and −11 ppm (Figure 11b). But the −6 ppm line remains intense and dominates the spectrum. This result along with the ^{27}Al MAS NMR observations suggests that at low P/Al ratio UHM-1 is constructed mainly of octahedral aluminum AlO_6 structural units and a small amount of hydroxylated phosphorus species.

^{29}Si MAS NMR. ^{29}Si MAS NMR spectra of a series of UHM-3 samples with variable Si/Al ratios are shown in Figure 12. At low Si/Al ratio only one resonance line around −87 ppm is resolved (Figure 12a). At increasing Si/Al ratio a second line around −94 ppm becomes resolvable (Figure 12b). The intensities of both lines increase with increasing Si/Al ratio, but the −94 ppm line increases relatively more and dominates the spectrum at a Si/Al ratio of 1.01 (Figure 12b−d). Based on literature reports on silicon-substituted aluminophosphate

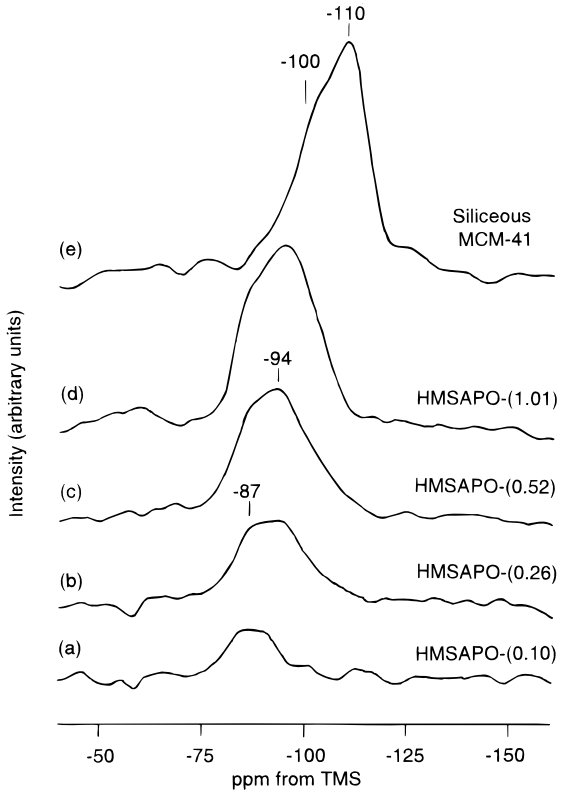

Figure 12. ^{29}Si MAS NMR spectra of as-synthesized silicoaluminophosphate samples (a) UHM-3-(0.10), (b) UHM-3-(0.26), (c) UHM-3-(0.52), and (d) UHM-3-(1.01). For comparison, (e) shows a typical ^{29}Si MAS NMR spectrum of siliceous MCM-41.

SAPO-*n* molecular sieves,[35,38] and considering the excess of aluminum over phosphorus in the UHM-3 materials and the high amount of substituted silicon, the −87 ppm line can be assigned to silicon coordinated through oxygen atoms to four

aluminum atoms as in $Si(OAl)_4$ structural units and the −94 ppm line to silicon in $Si(OAl)_3OSi$ units in which there exists a Si−O−Si linkage. This assignment is consistent with the observed spectroscopic change upon increasing silicon incorporation.

For comparison, Figure 12e shows a typical ^{29}Si MAS NMR spectrum from aluminosilicate MCM-41 materials in which the intense line around −110 ppm comes from $Si(OSi)_4$ structural units and the shoulder around −100 ppm from silicons in $Si(OSi)_3OH$ units.[24] The lack of these lines in the ^{29}Si MAS NMR spectra of UHM-3 materials suggests that islands of pure silicate MCM-41 phases can be ruled out. But the broad ^{29}Si MAS NMR line shape of UHM-3 similar to that of siliceous MCM-41 also suggests that the O−T−O angle varies somewhat in these UHM-3 materials, where T represents a Al, P, or Si tetrahedral atom.

Discussion

Synthesis of Aluminophosphate UHM-1 and Silicoaluminophosphate UHM-3. Sayari et al.[7−9] have successfully synthesized and characterized a series of layered aluminophosphate materials. They have also attempted to prepare mesoporous aluminophosphate materials with a three-dimensional structure by modifying the composition of the starting synthesis gels but report a lack of success.[8] On the basis of our results, we suggest that this is due to the use of Catapal alumina, low gel pH, high synthesis temperature, or some combination of these factors in agreement with a number of successful syntheses of tubular aluminophosphate mesoporous materials.[14−18]

Our synthesis for UHM-1 and UHM-3 has been performed in gels with a wide range of compositions and at variable temperature. However, the synthesis is successful only at room temperature in basic media within the following molar gel composition range: Al_2O_3:(0.6−3.4) P_2O_5:(0.0−1.0) SiO_2:(0.24−0.50) CTACl:(8.5−47.0) TMAOH:(200−642) H_2O. Higher temperature synthesis at 90 °C or over produces a well-defined but unstable lamellar phase. With variable gel composition, UHM-1 can be synthesized for a range of $CTACl/Al_2O_3$ ratios of 0.24−0.50, but at higher $CTACl/Al_2O_3$ ratios of 1−3 only amorphous material is formed. The P/Al molar ratio of the gels can be changed over a range of 0.6−3.4 without affecting the hexagonal structure of the products, which is different from a fixed P/Al ratio of 1.0 required for the synthesis of microporous aluminophosphate molecular sieves.[31] The addition of TMAOH is essential to the control of the gel pH at 8.5 or over for the formation of UHM-1; replacement of TMAOH with 0.1 M NaOH fails to form any mesoporous structures. Another factor that influences this synthesis is the aluminum source. The synthesis of UHM-1 and UHM-3 is successful with aluminum hydroxide and also aluminum isopropoxide[12] but not with Capatal alumina.[6−9]

Tubular Mesoporous Structures of Aluminophosphate UHM-1 and Silicoaluminophosphate UHM-3. All UHM-1 and UHM-3 samples exhibit a similar XRD pattern with one intense peak around 2.2° 2θ corresponding to a d spacing of about 40 Å and some other overlapped peaks in the range 3.0°−8.0° 2θ. On the basis of previous arguments for the disordered mesoporous materials KIT-1,[29] MSU-1 silica,[28] and an alumina phase,[30] such an XRD pattern corresponds to a three-dimensional, disordered network with short wormlike, tubular channels, which is different from but mimics a hexagonal MCM-41 mesopore structure. Therefore, the structural symmetry of these UHM-1 and UHM-3 materials is analogous to MSU-1 and KIT-1 rather than to a lamellar structure. This conclusion is well supported by the TEM images which show an array of disordered tubular channels about 40 Å in diameter.

The most reliable information about the mesopore structure of these UHM-1 and UHM-3 materials comes from N_2 adsorption experiments. The high BET specific surface areas up to 700 m^2/g upon heat treatment in flowing nitrogen at 400 °C strongly support the existence of a stable tubular mesoporous structure rather than a lameller structure. The small decrease in BET specific surface area upon heat treatment at 500 °C suggests that these materials are less thermally stable than siliceous MCM-41.

After complete decomposition of the organic structure-directing agent upon calcination in flowing oxygen at 500 °C, both UHM-1 and UHM-3 samples show a typical irreversible type IV adsorption isotherm with sharp inflections in the P/P_0 range from 0.45 to 0.75 and a broad H1 hysteresis loop. The P/P_0 position and the sharpness of this reflection confirm the presence of mesopores in UHM-1 and UHM-3, but the broad hysteresis loop reflects some mesopore disorder. This supports the XRD and TEM results that these UHM-1 and UHM-3 materials possess a disordered tubular mesopore structure like MSU-1 and KIT-1. The BJH plots for N_2 adsorption on these UHM-1 and UHM-3 samples reveal an average mesopore size of about 35 Å and a mesopore surface area (A_{BJH}) of 600 m^2/g, which together with XRD results suggest that the pore walls of these UHM-1 and UHM-3 materials are around 11 Å thick.

A comparison of UHM-1 and UHM-3 shows that UHM-3 exhibits a sharper inflection in its N_2 adsorption isotherm and a narrower pore size distribution than UHM-1. This indicates a less disordered mesoporous structure after silicon incorporation and suggests that the incorporation of silicon into UHM-1 facilitates the formation of a more regular aluminophosphate mesoporous structure.

Framework Atomic Arrangements in Aluminophosphate UHM-1 and Silicoaluminophosphate UHM-3. *Aluminophosphate UHM-1.* ^{27}Al and ^{31}P MAS NMR spectra reveal that UHM-1 with a relatively high P/Al ratio (0.60) is composed of AlO_4, AlO_6, and PO_4 structural units and hydroxylated phosphorus species. UHM-1 samples with lower P/Al ratios are constructed of relatively more AlO_6 structural units. Such mixed coordination environments in UHM-1 indicate that the condensation of either aluminum or phosphorus sources is incomplete and that these UHM-1 materials may have more disorder than siliceous MCM-41. On the other hand, this may suggest that AlO_4 and PO_4 structural units alone cannot easily form an ideal hexagonal mesoporous framework arrangement which is enforced by the surfactant assembly.

Silicoaluminophosphate UHM-3. For a quantitative evaluation of a series of UHM-3 samples, the relative amounts of tetrahedral aluminum and tetrahedral phosphorus in $P(OAl)_4$ structural units corresponding to the ^{31}P MAS NMR line at −19 ppm are calculated from the integrated signal intensity of each ^{27}Al or ^{31}P MAS NMR spectrum in Figures 8 and 9. The results are in Figure 13 as a plot versus the overall Si/(Si + Al + P) ratios from Table 1. Throughout the entire composition range these plots increase almost linearly but do not pass through the origin. It is apparent that the incorporation of silicon into UHM-1 to form UHM-3 causes a substantial increase of tetrahedral aluminum and tetrahedral phosphorus in more condensed $P(OAl)_4$ structural units even at very low silicon loading. Virtually all the aluminums are tetrahedral, and all the phosphorus are present as $P(OAl)_4$ structural units in UHM-3 after the silicon loading approaches a Si/Al ratio of unity. Since the ^{29}Si MAS NMR shows that the incorporated silicon is

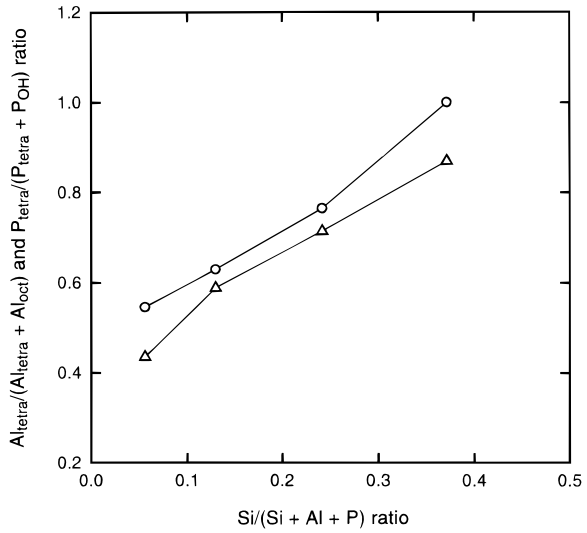

Figure 13. Plot of $Al_{tetra}/(Al_{tetra} + Al_{oct})$ (○) and $P_{tetra}/(P_{tetra} + P_{OH})$ (△) calculated from the integrated line intensities of the spectra in Figures 8 and 9, respectively, versus the Si/(Si + Al + P) ratios from Table 1 for silicoaluminophosphate UHM-3 samples.

atomically dispersed, it is suggested that the incorporation of silicon into UHM-3 promotes the formation of a more ordered framework arrangement similar to that in microporous silicoaluminophosphate molecular sieves.

A comparison of the coordination environments for silicon in microporous silicoaluminophosphate SAPO-*n* molecular sieves and in UHM-3 is of particular interest because it may provide some additional clues for elucidating the framework atomic arrangements in UHM-3 materials. SAPO-*n* contains tetrahedral arrangements of silicon, aluminum, and phosphorus via oxygen bridges between them. The silicon substitution into SAPO-*n* can be for (1) aluminum, (2) phosphorus, or (3) an aluminum−phosphorus pair. Flanigen et al.[38] suggested that mechanisms (2) and (3) are more likely than (1) for SAPO-*n* materials since they exhibit cation-exchange capacity and show an excess of aluminum over phosphorus. Davis et al.[35] further ruled out the possibility of silicon substitution by mechanism (3) because their ^{29}Si MAS NMR data for SAPO-37, which contains relatively more silicon ($Si_{0.125}Al_{0.51}P_{0.365}$) than other SAPO-*n* materials, show a single chemical environment for Si, which is inconsistent with more than one silicon environment expected for silicon substitution by mechanism (3).

UHM-3 also has excess aluminum over phosphorus and a substantial amount of silicon, and the ^{29}Si MAS NMR reveals two lines corresponding to two types of silicon environments, $Si(OAl)_4$ and $Si(OAl)_3OSi$, in which the second line develops for increasing Si/Al ratio (Figure 12). If we assume an ideal aluminophosphate UHM-1 framework with nearly unity P/Al, silicon substitution both by mechanisms (2) and (3) may occur. Silicon substitution by mechanism (2) creates $Si(OAl)_4$ structural units and by mechanism (3) creates $Si(OAl)_3OSi$ structural units.

Formation Mechanism of Aluminophosphate UHM-1 and Silicoaluminophosphate UHM-3. Crystalline silicate-based mesoporous M41S molecular sieves, in layered or hexagonal or cubic structures, are hydrothermally synthesized via a liquid crystal templating process using mostly long-chain cationic surfactant alkyltrimethylammonium salts as structure-directing agents.[1−3] The main steps in the synthesis involve the formation of a surfactant−silicate ion pair, their organization into a mesophase, and the condensation of silicate species to give inorganic layers or walls. The formation of these silicate-based mesoporous molecular sieves has been generalized as a self-assembly process involving electrostatic interactions between positively charged quaternary ammonium surfactants (S^+) and inorganic anions (I^-).[25,39,40] A neutral precursor assembly method involving hydrogen bonding between neutral amine surfactants (S^0) and neutral silica precursors (I^0) in alcohol−water solvent has also been demonstrated.[27,28] These concepts have been applied for the synthesis of other open-structure networks of various metal oxides.[39]

The synthesis of UHM-1 and UHM-3 materials is based on the self-assembly between a cationic surfactant (S^+) and an aluminophosphate precursor (I^-) in the presence of alkylammonium hydroxide. We postulate that the formation of UHM-1 and UHM-3 materials occurs by a modified S^+I^- ion pair process. The inorganic precursors (I^-) are aluminophosphate species of low polymerization degree with some hydroxyl groups. When an organic base TMAOH is added, the tetramethylammonium ion TMA^+ reacts with the hydroxyl group of these aluminophosphate species to produce a relatively weak ion pair ($I^-\cdots TMA^+$) since the TMA^+ cation has a large ionic radius. These ion pair species diffuse to the surfactant (S^+) assembly (micelle) interface and interact with the cationic surfactant headgroups. The interaction of the negative aluminophosphate species with the cationic surfactant headgroups is stronger than with the TMA^+ cation. The micellar structure then organizes the condensation and polymerization of adjacent aluminophosphate species to form an ordered tubular mesostructure.

The function of the organic ammonium cation from TMAOH seems to be to modify the strength of the electrostatic interaction between the aluminophosphate species and the cationic surfactant micelle assembly to form a $S^+I^-\cdots TMA^+$ ion pair. If NaOH is used, the Na^+ cation with a smaller ionic radius than TMA^+ has a stronger ion pair interaction with the aluminophosphate species and prevents sufficient interaction with the cationic surfactant assembly. Thus, the assembly of mesostructural aluminophosphate fails. The aluminum source also seems critical. Aluminum hydroxide may form a less polymerized aluminophosphate with many hydroxyl groups and favor the assembly of the mesostructure compared to Capatal alumina.

Conclusions

Tubular mesoporous aluminophosphate UHM-1 and silicoaluminophosphate UHM-3 molecular sieves have been synthesized via a liquid crystal templating process in the presence of a cationic surfactant. We show that this synthesis can be performed over a broad range of gel composition but is successful only at room temperature in basic media by addition of an organic base. The solid products from the gels are relatively thermally stable and possess disordered tubular channels of about 40 Å in diameter. The UHM-1 materials have a nonideal aluminophosphate framework due to incomplete condensation of phosphorus species so that both tetrahedral and octahedral aluminum are present. Phosphorus is present in a tetrahedral environment and also as hydroxylated species. The incorporation of silicon into UHM-1 to form UHM-3 induces flexibility into the mesoporous aluminophosphate framework enforced by the organic surfactant assembly and promotes more complete condensation between aluminum, phosphorus, and silicon via oxygen bridges. This facilitates the formation of the aluminophosphate-based mesoporous structure.

Acknowledgment. This research was supported by the Robert A. Welch Foundation, the University of Houston Energy Laboratory, and the National Science Foundation.

References and Notes

(1) Kresge, C. T.; Leonowicz, M. E.; Roth, W. J.; Vartuli, J. C.; Beck, J. S. *Nature* **1992**, *359*, 710.

(2) Beck, J. S.; Vartuli, J. C.; Roth, W. J.; Leonowicz, M. E.; Kresge, C. T.; Schmitt, K. D.; Chu, C. T.-W.; Olson, D. H.; Sheppard, E. W.; McCullen, S. B.; Higgins, J. B.; Schlenker, J. L. *J. Am. Chem. Soc.* **1992**, *114*, 10834.

(3) Chen, C.-Y.; Burkett, S. L.; Li, H.-X.; Davis, M. E. *Microporous Mater.* **1993**, *2*, 27.

(4) Sayari, A. *Chem. Mater.* **1996**, *8*, 1840.

(5) Wilson, S. T.; Lok, B. M.; Messina, C. A.; Cannan, T. R.; Flanigen, E. M. *J. Am. Chem. Soc.* **1982**, *104*, 1146.

(6) Oliver, S.; Kuperman, A.; Coombs, N.; Louth, A.; Ozin, G. A. *Nature* **1995,** *378*, 47.

(7) Sayari, A.; Karra, V. R.; Reddy, J. S.; Moudrakovski, I. L. *J. Chem. Soc., Chem. Commun.* **1996,** 411.

(8) Sayari, A.; Moudrakovski, I. L.; Reddy, J. S. *Chem. Mater.* **1996**, *8*, 2080.

(9) Sayari, A. In *Progress in Zeolite Microporous Materials*; Chon, H., Ihm, S.-K., Uh, Y. S., Eds.; Studies in Surface Science and Catalysis Vol. 105; Elsevier: Amsterdam, 1997; pp 37−44.

(10) Gao, Q.; Chen, J.; Xu, E.; Yue, Y. *Chem. Mater.* **1997**, *9*, 457.

(11) Gao, Q.; Chen, J.; Li, S.; Xu, R. In *Progress in Zeolite Microporous Materials*; Chon, H., Ihm, S.-K., Uh, Y. S., Eds.; Studies in Surface Science and Catalysis Vol. 105; Elsevier: Amsterdam, 1997; pp 389−396.

(12) Cheng, S.; Tzeng, J.-N.; Hsu, B.-Y. *Chem. Mater.* **1997**, *9*, 1788.

(13) Pophal, C.; Schnell, R.; Fuess, H. In *Progress in Zeolite Microporous Materials*; Chon, H., Ihm, S.-K., Uh, Y. S., Eds.; Studies in Surface Science and Catalysis Vol. 105; Elsevier: Amsterdam, 1997; pp 101−108.

(14) Zhao, D.; Luan, Z.; Kevan, L. *J. Chem. Soc.,Chem. Commun.* **1997**, 1009.

(15) Zhao, D.; Luan, Z.; Kevan, L. *J. Phys. Chem. B* **1997**, *101*, 6943.

(16) Kimura, T.; Sugahara, Y.; Kuroda, K. 11th International Zeolite Conference, Abstract RP45, Seoul, Korea, 1996.

(17) Chakraborty, B.; Pulikottil, A. C.; Das, S.; Viswanathan, B. *J. Chem. Soc., Chem. Commun.* **1997,** 911.

(18) Feng, P.; Xia, Y.; Feng, J.; Bu, X.; Stucky, G. D. *J. Chem. Soc., Chem. Commun.* **1997,** 949.

(19) Holland, B. T.; Isbester, P. K.; Blanford, C. F.; Munson, E. J.; Stein, A. *J. Am. Chem. Soc.* **1997,** *119*, 6796.

(20) Tanev, P. T.; Vlaev, L. T. *J. Colloid Interface Sci.* **1993**, *160*, 110.

(21) Luan, Z.; He, H.; Zhou, W.; Cheng, C.-F.; Klinowski, J. *J. Chem. Soc., Faraday Trans.* **1995**, *91*, 2955.

(22) Blackwell, C. S.; Patton, R. L. *J. Phys. Chem.* **1984**, *88*, 6135.

(23) Maistriau, L.; Gabelica, Z.; Derouane, E. G.; Vogt, E. T. C.; van Oene, J. *Zeolites* **1991**, *11*, 583.

(24) Luan, Z.; Cheng, C.-F.; Zhou, W.; Klinowski, J. *J. Phys. Chem.* **1995**, *99*, 1018.

(25) Monnier, A.; Schüth, F.; Huo, Q.; Kumar, D.; Margolese, D.; Maxwell, R. S.; Stucky, G. D.; Krishnamurthy, M.; Petroff, P.; Firouzi, A.; Janicke, M.; Chmelka, B. F. *Nature* **1993**, *261*, 1299.

(26) Barrett, E. P.; Joyner, L. G.; Halenda, P. P. *J. Am. Chem. Soc.* **1951**, *73*, 373.

(27) Tanev, P. T.; Pinnavaia, T. J. *Science* **1995**, *267***,** 865.

(28) Bagshaw, S. A.; Prouzet, E.; Pinnavaia, T. J. *Science* **1995,** *269*, 1242.

(29) Ryoo, R.; Kim, J. M.; Ko, C. H.; Shin, C. H. *J. Phys. Chem.* **1996,** *100*, 17718.

(30) Vaudry, F.; Khodabandeh, S.; Davis, M. E. *Chem. Mater.* **1996,** *8*, 1451.

(31) Szostak, R. In *Molecular Sieves, Principles of Synthesis and Identification*; Van Nostrand Reinhold: New York, 1989; pp 253−276.

(32) Sing, K. S. W.; Everett, D. H.; Haul, R. A. W.; Moscow, L.; Pierotti, R. A.; Rouquerol, J.; Siemieniewska, T. *Pure Appl. Chem.* **1985**, *57*, 603.

(33) Müller, D.; Fahlke, J. B.; Ladwig, G. *Zeolites* **1985**, *5*, 53.

(34) Rocha, J.; Kolodziejski, W.; He, H.; Klinowski, J. *J. Am. Chem. Soc.* **1992**, *114*, 4884.

(35) de Saldarriaga, L. S.; Saldarriaga, C.; Davis, M. E. *J. Am. Chem. Soc.* **1987**, *109*, 2686.

(36) Barrie, P. *Spectroscopy of New Materials;* Wiley: New York, 1993; p 151.

(37) Barr, T. L.; Klinowski, J.; He, H.; Alberti, K.; Müller, G.; Lercher, J. *Nature* **1993**, *365*, 429,

(38) Lok, B. M.; Messina, C. A.; Patton, R. L.; Gajek, R. T.; Cannan, T. R.; Flanigen, E. M. *J. Am. Chem. Soc.* **1984**, *106*, 6092.

(39) Huo, Q.; Margolese, D. I.; Cielsa, U.; Feng, P.; Gier, T. E.; Sieger, P.; Leon, R.; Petroff, P. M.; Schüth, F.; Stucky, G. D. *Nature* **1994**, *368***,** 317.

(40) Huo, Q.; Margolese, D. I.; Cielsa, U.; Demuth, D. G.; Feng, P.; Gier, T. E.; Sieger, P.; Firouzi, A.; Chmelka, B. F.; Schüth, F.; Stucky, G. D. *Chem. Mater.* **1994,** *6*, 1176.